J Bionic Eng 15 (2018) 260–269
DOI: https://doi.org/10.1007/s42235-018-0020-1

Journal of Bionic Engineering
http://www.springer.com/journal/42235

Energy Analysis of a CPG-controlled Miniature Robotic Fish

Junzhi Yu[1*], Shifeng Chen[1,2], Zhengxing Wu[1], Xingyu Chen[1,2], Ming Wang[3]

1. *State Key Laboratory of Management and Control for Complex Systems*, *Institute of Automation*, *Chinese Academy of Sciences*, *Beijing* 100190, *China*
2. *University of Chinese Academy of Sciences*, *Beijing* 100049, *China*
3. *School of Information and Electrical Engineering*, *Shandong Jianzhu University*, *Jinan* 250101, *China*

Abstract

Bionic robotic fish has a significant impact on design and control of innovative underwater robots capable of both rapid swimming and high maneuverability. This paper explores the relationship between Central Pattern Generator (CPG) based locomotion control and energy consumption of a miniature self-propelled robotic fish. To this end, a real-time energy measurement system compatible with the CPG-based locomotion control is firstly built on an embedded system. Then, tests are conducted on the untethered actual robot. The results indicate that different CPG feature parameters involving amplitude, frequency, and phase lag play distinct roles in energy consumption under different swimming gaits. Specifically, energy consumption is positively correlated with the changes in the amplitude and frequency of CPGs, whereas the phase lag of CPGs has little influence on the energy consumption. It may offer important inspiration for improving energy efficiency and locomotion performance of versatile swimming gaits.

Keywords: bionic robotic fish, energy analysis, Central Pattern Generator (CPG), swimming, motion control

1 Introduction

Research on bionic swimming robots has considerably expanded in recent years. On the one hand, marine organisms have evolved amazing motion skills over millions of years, offering a multitude of design options in highly dynamic aquatic environments[1–4]. On the other hand, integrating biological features into robotic systems creates significant opportunities for enhanced understanding of physical principles of aquatic propulsion and maneuvering. Replicating motion modes or characteristics of marine organisms, as a consequence, has become an innovative and controllable platform in the context of bio-robotics. As a good example, fish-inspired swimming robots, i.e., bionic robotic fish, have shown excellent performance in efficient propulsion and high maneuverability as opposed to traditional underwater vehicles propelled by screw-type thrusters. The research on bionic robotic fish not only provides a repeatable verification platform for biological investigation, but has also witnessed a multitude of applications such as underwater exploration, oceanography, archaeology, search and rescue, patrol, marine environmental monitoring, and mobile sensing, where operations are unsafe or impractical for divers or conventional underwater vehicles[5–11].

Locomotion control is a fundamental issue for development and operation of various robots, especially in dynamic underwater environments. Faster speed and higher maneuverability of robotic fish demand an increased understanding of the complex interaction between locomotion mechanisms and surrounding fluids. Meanwhile, this requirement motivates the development of new theoretical results in adaptive and robust control, which in turn enhances locomotion capability and expands robotic applications. With regard to the locomotion control of robotic fish, there are two methods, i.e., body wave-based swimming control and Central Pattern Generator (CPG)-based control method[12]. The former relies on the mimicry of a traveling fish body wave featuring a curvature of the spine and muscle with increasing amplitude, whereas the latter is inspired by a neural control mechanism. Specifically, CPGs can be interpreted as a dedicated neural mechanism involving a

***Corresponding author:** Junzhi Yu
E-mail: junzhi.yu@ia.ac.cn

group of neurons that coordinately generates rhythmic signals without sensory feedback, while sensory feedback is needed to shape the CPG signals[13,14]. Biological CPGs are radically responsible for producing rhythmic movements such as locomotion, breathing, chewing, scratching, and flying. The well-established artificial CPG model can support smooth oscillation transitions, corresponding to different rhythmic motions exhibited in animals. In brief, CPG that features strong robustness, excellent adaptability, as well as easily adjustable output signals, is well suited to robot control involving multi-articulate or multiple degrees of freedom-related cases. By contrast with the conventional body wave-based swimming control method, the CPG-based control method only needs to adjust output signals' characteristics and keep them smooth and continuous even if parameters are drastically changed.

With such distinct advantages, the CPG-based control method is widely employed to generate a wide range of swimming gaits such as forward swimming, backward swimming, turning, diving and surfacing. For instance, Zhang *et al.* proposed a bionic neural network comprising a high level controller and a chain of CPGs to yield fishlike motions[15,16]; Wu *et al.* implemented flexible and precise turning motions in both fishlike forward and backward swimming by use of CPG-based control and closed-loop orientation control strategy[17]; Li *et al.* used a three-link robotic fish to demonstrate the proposed general CPG network running on the microcontroller[18]; Yu *et al.* utilized a combination of dynamic model and particle swarm optimization to optimize the CPG characteristic parameters for enhanced propulsive performance in both forward and backward swimming[19]; Staffa *et al.* presented a modeling framework allowing developers to model simple CPG-controlled robotic systems for regulating the sensor-motor loops[20]. Ge *et al.* performed an in-depth comparative analysis of the prediction mean-squared error, the filter-calculated mean-squared error, and the gain matrix for the extended strong tracking filter and strong tracking filter for better tracking performance[21,22]. However, these studies seldom consider the impact of energy consumption in the CPG-based locomotion control. In fact, energy consumption is a crucial factor for battery-powered robots, because reduced energy consumption often corresponds to prolonged lifetime on one charge. As a consequence, it is worthwhile to explore the energy consumption issue of bionic robotic fish in close relation to the applied control methods.

In this work, we report the relationship between the CPG-based locomotion control and energy consumption of a fully untethered two-joint robotic fish. To directly measure the energy consumption, a real-time energy measurement system is developed and integrated into the embedded control system. Analyses of data on actual energy consumption indicate different roles of the CPG feature parameters in different swimming gaits. To the best of our knowledge, no systematic empirical research on CPG-related swimming energy consumption exists. The obtained results will potentially guide energy optimization and control update for efficient locomotion control in dynamic aquatic environments.

The remainder of this paper is organized as follows. We start by offering an overview of the mechatronic design and the CPG-based locomotion control for the miniature self-propelled robotic fish in section **2**. Testing results and discussion are provided in section **3**. Finally, section **4** gives some concluding remarks.

2 Materials and methods

This section presents an overall CPG-controlled robotic fish system along with the data acquisition system for on-site measurement of energy consumption of moving joints.

2.1 Mechatronic design of robotic fish

To establish a fish-inspired robotic platform for popular science education and public exhibition, a fully untethered miniature robotic fish has been developed[23]. The morphology of the robotic fish is modeled after shark, which affords sufficient space for mechatronic parts. As shown in Fig. 1, the robot is composed of a shark-shaped head shell, a flexible posterior body with two active joints, a caudal fin, and a black compliant outer skin. Functionally, the rigid head shell accommodates a pair of mechanical pectoral fins, multiple sensors, control circuits, a rechargeable lithium battery pack, and a duplex wireless communication module. The two-joint posterior body connected by the caudal fin serves as the main thruster for propulsion and maneuvering, while the

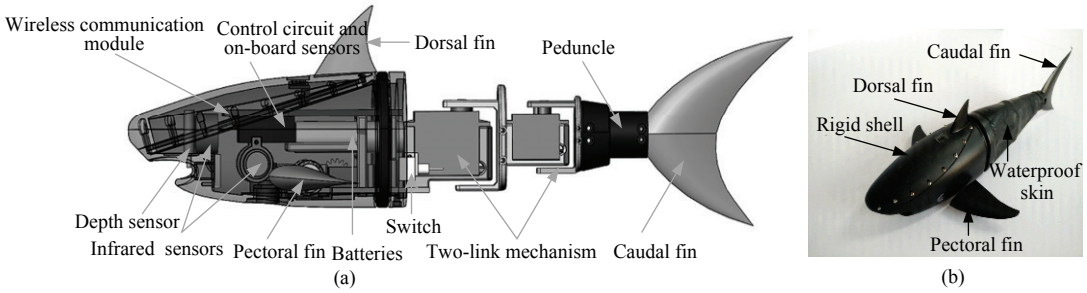

Fig. 1 Mechanical design of the robotic fish. (a) Conceptual design; (b) robotic prototype.

Table 1 Technical specification of the developed robotic prototype

Items	Characteristics
Dimension ($L\times W\times H$)	35 cm × 6.1 cm × 8.3 cm
Weight	970 g
Number of joints	2
Actuator	Servo (HS-5565MH, HS-82MG)
Controller	STM32F407
Control mode	Wireless or autonomous mode
Operation time	Approx. 1 h

mechanical pectoral fin pair is used for maneuvering and assistive propulsion. The coordinated motion of the posterior body, caudal fin, and pectoral fins endows the robotic fish with the ability to perform multimodal swimming gaits, such as forward swimming, backward swimming, submerging/surfacing, and turning. The compliant outer skin made of lactoprene serves to protect the structures from water and also to reduce fluid drag to some extent[24]. By properly placing clump weights, mass distribution of the robotic fish can be balanced for relatively stable 3D motions. Density of the robotic fish, in particular, has to be calibrated close to water so that a neutrally buoyant state can initially be achieved. The resulting robotic prototype is depicted in Fig. 1b, which measures 35 cm long, 6 cm wide (maximum, at the shoulder), 8 cm high (maximum, at the shoulder) and weighs approximately 970 g in total. Table 1 further lists technical specification of the developed robotic prototype.

As for electronics and sensors used in the robotic fish, a hybrid control system with embedded microcontroller STMicroelectronics STM32F407 is built. At present, available on-board sensors include a gyroscope, a depth sensor, two light sensors, three infrared sensors, and a coulomb sensor. The main function of the embedded microcontroller is multi-sensor data processing, locomotion control, and bi-directional radio communication between the robot and the upper console. Specifically, as will be detailed later, the locomotion control of the miniature robotic fish is governed by a bio-inspired CPG controller. With the aid of STM32F407-centered embedded system, the CPG controller can be solved in real time and corresponding pulse width modulation signals subsequently output for actuators, i.e., servos, enabling various motion control requirements.

2.2 CPG-based locomotion control

Considering that the swimming robotic fish can be treated as an oscillating serial mechanism coupled with a pectoral fin pair, a CPG network agreeing well with the propulsive configuration is employed. The multi-joint fish body, functionally similar to the spinal cord in a biological neural system, is governed by N coupled oscillators. In this work, a Hopf oscillator-based CPG model is utilized. By means of adjacent coupling, the CPG can be reduced with significantly fewer parameters, which are used to adjust the amplitudes, frequencies, and phase lags of output signals. Analogous to muscles reacting to neural signals, an output transition function is imported to transform the oscillating CPG signals to motor driving signals.

The detailed CPG model is described as:

$$\begin{cases} \dot{x} = -\omega_i y_i + x_i(A_i - x_i^2 - y_i^2) + h_1(x_{i-1}\cos\psi_i + y_{i-1}\sin\psi_i) \\ \dot{y} = \omega_i x_i + y_i(A_i - x_i^2 - y_i^2) + h_2(x_{i+1}\sin\psi_{i+1} + y_{i+1}\cos\psi_{i+1}) \end{cases}, \quad (1)$$

where the subscript i indicates the i-th oscillator in the CPG network ($i = 1, 2, \ldots, N$). x_i and y_i represent the sate variables of the i-th oscillating neurons. ω_i and A_i are the

intrinsic oscillation frequency and amplitude, where $\omega_i = 2\pi f_i$ (f_i denotes the oscillation frequency of the i-th joint in Hz). ψ_i is the phase lag of output signal. h_1 and h_2 are positive constants of the coupling strength.

An output transition function Eq. (2) is then defined to transform the CPG output signal to the actuator control signal.

$$z_{\text{out}}[i] = y[i] \times c \times ratio[i] + mid[i], \tag{2}$$

where $z_{\text{out}}[i]$ and c represent respectively the output signal of the i-th CPG and the magnification coefficient. $ratio[i]$ is a coefficient converting CPG data to the position of servo motor. $mid[i]$ is the middle value of the servo motor.

Through adjusting the feature parameters of CPG control, ω_i and A_i, the speed of the robotic fish can be changed in forward swimming. By adding different deflections to symmetric swimming gaits, the robotic fish is able to perform turning motions. If not otherwise specified, the assumptions that $\omega_i = \omega$ and $\psi_i = \psi$ are constant for all oscillators hold in the CPG-based locomotion control.

2.3 Energy measurement system

Energy measurement is the first step towards energy analysis and performance optimization. Practically, energy consumption is related to many parts in the robotic fish, like circuit, sensors, and moving joints. Since the oscillating posterior body and caudal fin offer the main thrust for propulsion, most of the energy is consumed by driving motors. Moreover, considering that most of CPGs seem to be either reorganized or distributed circuits, the power consumed by actuators is recorded to gain a direct connection between the CPGs and the actuation system. A special focus is then placed on the current, voltage, and instantaneous power of driving motors to explore the relationship between the energy consumption and CPG feature parameters in steady swimming.

To acquire the data of current and voltage, a real-time energy measurement system is designed, as shown in Fig. 2. Voltage can be sampled by Analog-to-digital converter (ADC), whereas current hardly be directly attained, which can be calculated by using Ohm's law. The value of resistance, naturally, become the key factor in the system. The output current will be confined, if its value is quite high. On the contrary, signal amplification and sensibility will be impacted. Meanwhile, sampling precision is another key point, due to simultaneous sampling for multicenter. The sampling precision of the chosen chip MAX11331 is 10 bits or 12 bits. The maximal sampling rate of the chip is 3 MSPS, and the number of its sampling channel is no less than 16. For the robotic fish developed in this work, data in no more than 8 channels can be acquired simultaneously via SPI interface, which can work in both inner-clock mode and external-clock mode. The SPI interface supports both single-channel-sampling and programmable channel-ordered-sampling. Furthermore, its working power is quite low, whose maximum is 15.2 mW. As an external reference source, MAX6133-3.0 is used, and two resistances valued by 100 K and 200 K are used for voltage matching, due to the different voltage levels between steering motor and ADC, whose values are 6 V and 3 V, respectively. A 0.01 Ω resistance is used in circuit trunk for current measurement. Thus, the current will be amplified by the current-sampling chip MAX4172. To avoid the variety of current impacted by ADC, an operational amplifier LM4172 is employed, which is responsible for the isolation between sampling interface and output interface. As a result, the voltage acquired by ADC, i.e., the output of MAX4172, can be obtained.

At the level of software design, embedded software and upper-computer software are developed. The former includes MAX11331 driver, program of data acquisition, and wireless communication. A 16-bit-long SPI interface is used as transfer protocol for MAX11331, which

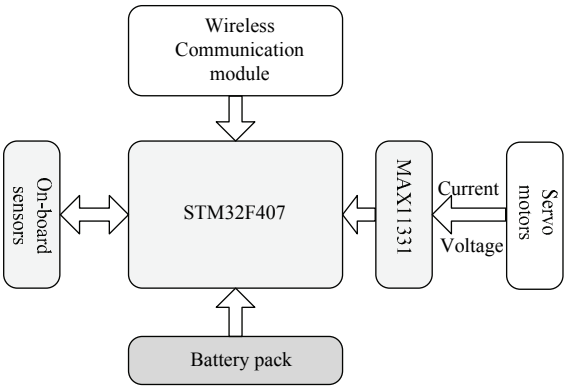

Fig. 2 The structure of energy measurement system.

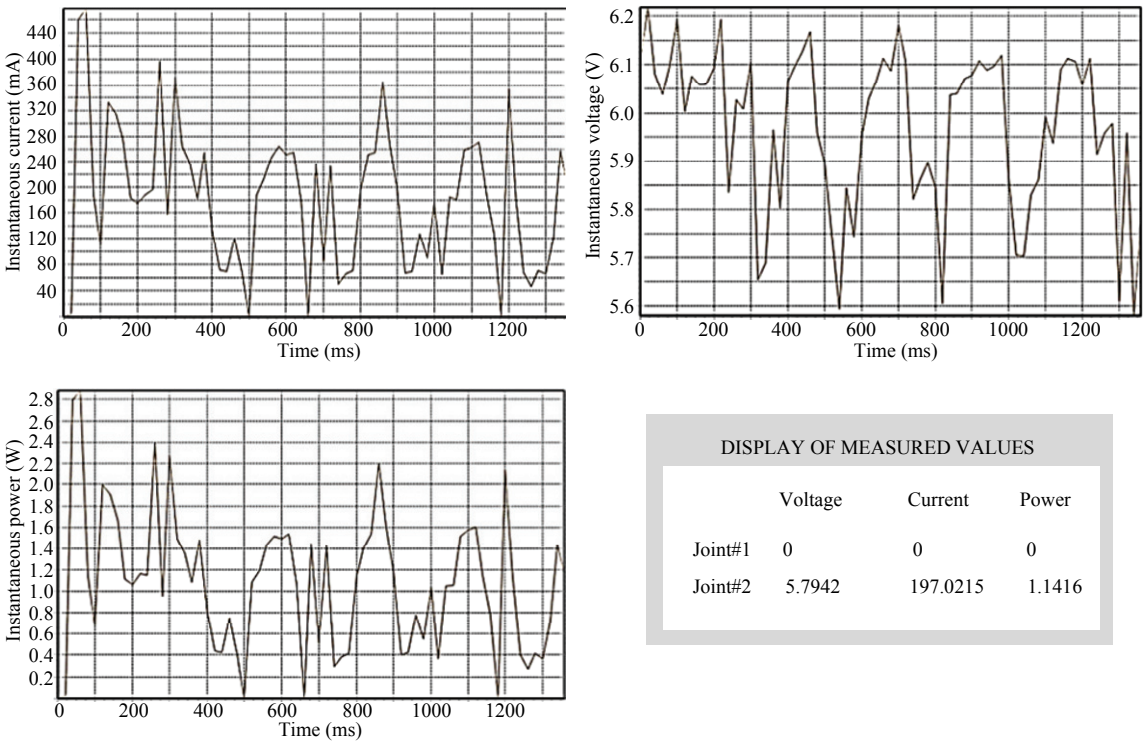

Fig. 3 A snapshot of the sampling data display console.

can work in both inner-clock mode and external-clock mode. The latter primarily receives real-time energy-related data via wireless module and display them by TeeChart, which is a kind of graph tool developed by Steema Software SL company. Fig. 3 shows a snapshot of the sampling data display console in operation.

3 Results and discussion

In this section, aquatic experiments on the actual two-joint CPG-governed robotic fish were conducted in indoor pool with calm water. The dimension of the pool is 5 m long, 4 m wide, and 1.5 m deep. The water temperature was about 20 ˚C. Particular emphasis was placed on the energy consumption of steady swimming under different CPG feature parameters. The experiments adopted control variate method. Regarding three factors in the CPG model, i.e., amplitude (A_i), frequency (ω_i), and phase lag (ψ_i), when a specific parameter is analyzed, another two variables maintain constant. For the measurement of power, the real-time detection of current and voltage eventually works. It should be noted that, although driving motors share the same 6 V power supply, their current and voltage characteristics are not completely same, due to inconsistent motor properties.

The first experiment concerned the amplitude effect on the energy consumption. In principle, the amplitude A_i in the CPG model directly influences the oscillatory amplitude of moving joints, accompanied by the alteration of speed and energy consumption. Through sensing instantaneous current and voltage, instantaneous power of each joint can ultimately be measured under conditions of varying amplitude. At present, the robotic fish has five swimming gaits, i.e., advancing, surfacing, diving, left turning, and right turning. The energy consumption in surfacing and diving is similar to that in advancing, since these two gaits primarily depend on variable angle of attack caused by pectoral fins while the motion mode of caudal fin in surfacing and diving agrees with that in advancing. Therefore, it is reasonable to merely consider energy consumption cases of advancing, left turning, and right turning. Through altering amplitude in different gaits, the relationship between energy consumption and amplitude was explored. To be specific, under conditions of constant frequency and phase lag, i.e., $\omega = 22$ and $\psi = 0^{\circ}$, five groups of amplitudes were tested. The initial amplitudes were set as $A_1 = 10.7032$

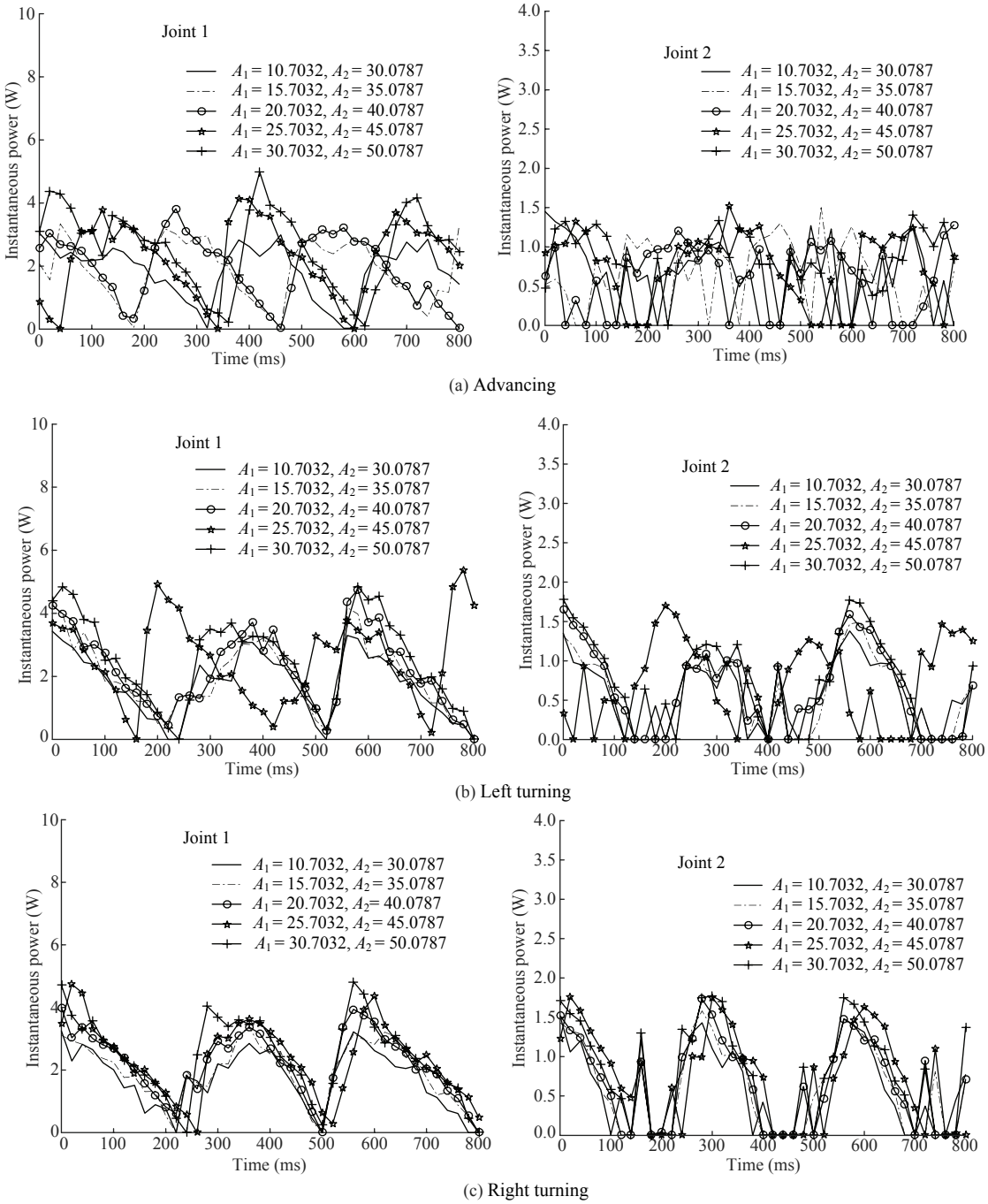

Fig. 4 The power consumption versus amplitude in the gaits of advancing, left turning, and right turning.

and $A_2 = 30.0787$ with an increment of 5. Fig. 4 plots the power consumption versus amplitude in the gaits of advancing, left turning, and right turning, respectively. As can be observed, three tested gaits exhibit similar trend. That is, the energy consumption of each joint increases with amplitude over the whole testing range.

The next experiment was on the frequency impact. Besides amplitude factor, increased swimming speed is generally accompanied by large increase in the frequency of CPG model. In tests, when amplitude and phase lag were fixed, i.e., $A_1 = 25.7032$, $A_2 = 45.0787$, and $\psi = 0^\circ$, five groups of frequencies were examined. Specifically, the starting frequency was set as $\omega = 22$

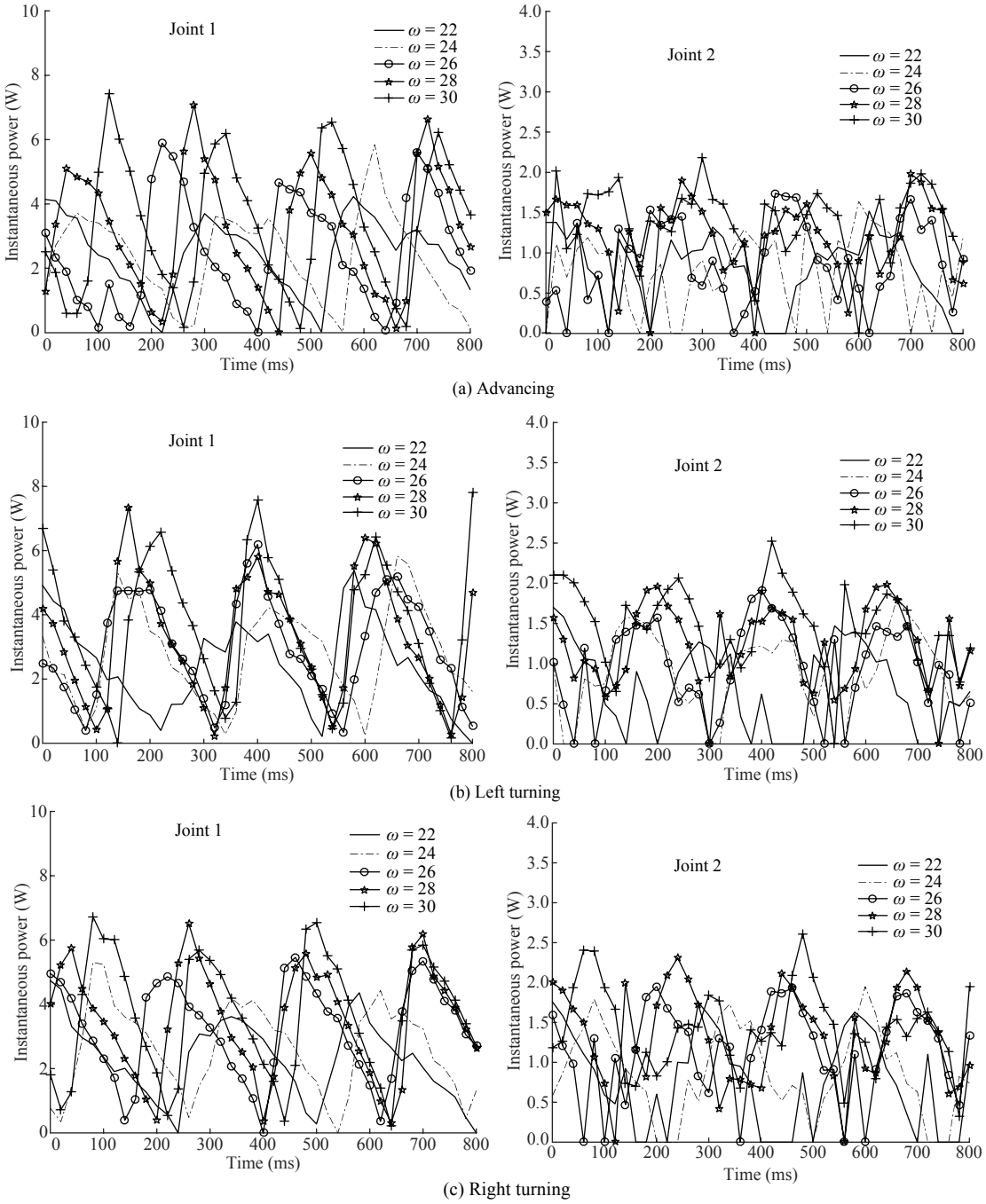

Fig. 5 The power consumption versus frequency in the gaits of advancing, left turning, and right turning.

with a step of 2. The power versus frequency curve in the gaits of advancing, left turning, and right turning is illustrated in Fig. 5. As can be seen, the graphs show a general tendency towards higher energy consumption with larger frequency.

The third experiment was performed to evaluate the effect of phase lag on the energy consumption for different swimming gaits. For the used CPG model, phase lag has a role to play in coordinating multiple moving joints, which directly affects propulsive speed of robotic fish. However, in terms of energy consumption, phase lag has little influence as opposed to other two CPG parameters. The main reason is that phase lag is only associated with the arriving time to a specific position

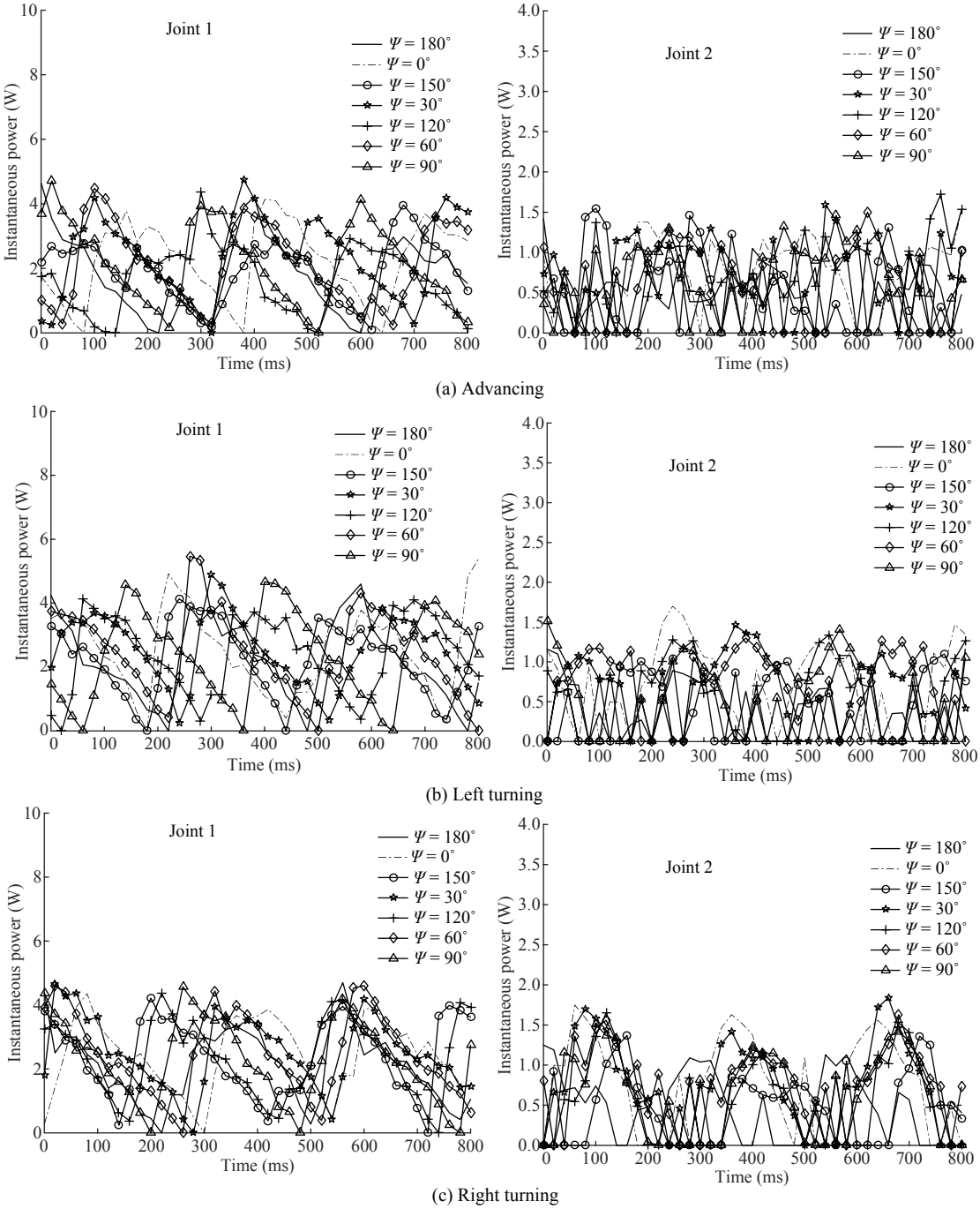

Fig. 6 The power consumption versus phase lag in the gaits of advancing, left turning, and right turning.

whereas the consumed energy at each waypoint is almost identical. To verify this supposition, seven testing cases with fixed amplitude and frequency (i.e., A_1 = 25.7032, A_2 = 45.0787, and ω = 22) were considered. The initial phase lag was set as ψ = 0° with a step of 30°. Fig. 6 shows the experimental results on energy consumption versus phase lag. After careful scrutiny, it could be found that there were some differences between the first joint and the second joint with respect to average power. But on the whole, there was no substantial difference of energy consumption for each joint among the seven phase lags. Apparently, the obtained result is almost consistent with the theoretical analysis.

Table 2 Average power consumed by two oscillating joints under different testing conditions (Unit: W)

Testing conditions	Advancing	Left turning	Right turning
$A_1 = 10.7032$, $A_2 = 30.787$	1.27	1.17	1.17
$A_1 = 15.7032$, $A_2 = 35.787$	1.26	1.28	1.29
$A_1 = 20.7032$, $A_2 = 40.787$	1.28	1.45	1.44
$A_1 = 25.7032$, $A_2 = 45.787$	1.51	1.64	1.57
$A_1 = 30.7032$, $A_2 = 50.787$	1.70	1.64	1.63
$\omega = 22$	1.62	1.58	1.53
$\omega = 24$	1.57	1.84	1.74
$\omega = 26$	1.71	1.95	2.20
$\omega = 28$	2.20	2.23	2.41
$\omega = 30$	2.36	2.58	2.54
$\psi = 180^\circ$	1.17	1.32	1.30
$\psi = 0^\circ$	1.47	1.62	1.59
$\psi = 150^\circ$	1.23	1.36	1.45
$\psi = 30^\circ$	1.54	1.59	1.64
$\psi = 120^\circ$	1.18	1.46	1.44
$\psi = 60^\circ$	1.38	1.57	1.64
$\psi = 90^\circ$	1.40	1.48	1.47

Furthermore, Table 2 tabulates the data on the average power under different conditions of amplitude, frequency, and phase lag, offering a better understanding of power difference. Again, in exploring the relationship between propulsive characteristics and energy consumption of fishlike swimming, the CPG model with explicit control parameters offers a feasible and convenient alternative to separate determination of energy role for each feature parameter. In reality, battery powered robotic fish might have to be confined to limited duration because of battery constraints. However, it is possible to achieve energy efficiency through behavior change with minimum energy expenditure. Hence, how to effectively link low energy consumption corresponding to a CPG control parameter set is a topic worthy of further investigation[25,26]. It will provide new clues for understanding energy-saving swimming behaviors and their control mechanisms. In addition, energy-based hybrid control framework for Hamiltonian systems may be transferred to the swimming control of robotic fish from the standpoint of cybernetics.

4 Conclusion and future work

In this paper, we design a miniature self-propelled CPG-controlled robotic fish as well as its energy measurement system. Based on the developed fishlike propulsion platform, the relationship between CPG-based locomotion control and energy consumption of robotic fish is first explored by means of the control variate method. Specifically, three CPG feature parameters and three typical swimming gaits are examined. It is found that energy consumption is positively correlated with the changes in amplitude and frequency, while phase lag has little impact on the energy consumption. The obtained results will shed light on the understanding of energy-saving swimming behaviors, control mechanisms, as well as their coordinated optimization.

In the near future, we will concentrate on energy optimization of multimode swimming gaits. Particularly, how to develop an optimization algorithm with a low time cost and global optimum and integrate it into the CPG-based locomotion control remains challenging. Meanwhile, energy-based hybrid control will be investigated to acquire better energy efficiency for those bionic underwater robots under realistic dynamic environments. Specifically, new methods employing Hamiltonian formulation of mechanics for creation of nonlinear dynamic models of robotic structures would be beneficial to efficient locomotion control[27–29].

Acknowledgment

This work was supported by the National Natural Science Foundation of China (Nos. 61725305, 61573226, 61763042, 61663040) and the Beijing Natural Science Foundation (Nos. 4161002, 4164103).

References

[1] Fish F E. Advantages of natural propulsive systems. *Marine Technology Society Journal*, 2013, **47**, 37–44.

[2] Tan X. Autonomous robotic fish as mobile sensor platforms: Challenges and potential solutions. *Marine Technology Society Journal*, 2011, **45**, 31–40.

[3] Yu J, Wen L, Ren Z. A survey on fabrication, control, and hydrodynamic function of biomimetic robotic fish. *Science China Technological Sciences*, 2017, **60**, 1365–1380.

[4] Kwak B, Bae J. Toward fast and efficient mobility in aquatic environment: A robot with compliant swimming appendages inspired by a water beetle. *Journal of Bionic Engineering*, 2017, **14**, 260–271.

[5] Liang J, Wang T, Wen L. Development of a two-joint robotic fish for real-world exploration. *Journal of Field Robotics*, 2011, **28**, 70–79.

[6] F. Shen, C. Wei, Z. Cao, C. Zhou, D. Xu, W. Zhang. Water quality monitoring system based on robotic dolphin. *Proceedings of World Congress on Intelligent Control and Automation*, Taipei, China, 2011, 243–247.

[7] Yan Q, Wang L, Liu B, Yang J, Zhang S. A novel implementation of a flexible robotic fin actuated by shape memory alloy. *Journal of Bionic Engineering*, 2012, **9**, 156–165.

[8] Hu T, Low K H, Shen L, Xu X. Effective phase tracking for bioinspired undulations of robotic fish models: A learning control approach. *IEEE/ASME Transactions on Mechatronics*, 2014, **19**, 191–200.

[9] Ryuh Y S, Yang G H, Liu J, Hu H. A school of robotic fish for mariculture monitoring in the sea coast. *Journal of Bionic Engineering*, 2015, **12**, 37–46.

[10] Zhang S, Qian Y, Liao P, Qin F, Yang J. Design and control of an agile robotic fish with integrative biomimetic mechanisms. *IEEE/ASME Transactions on Mechatronics*, 2016, **21**, 1846–1857.

[11] Wu Z, Liu J, Yu J, Fang H. Development of a novel robotic dolphin and its application to water quality monitoring. *IEEE/ASME Transactions on Mechatronics*, 2017, **22**, 2130–2140.

[12] Yu J, Wang K, Tan M, Zhang J. Design and control of an embedded vision guided robotic fish with multiple control surfaces. *The Scientific World Journal*, 2014, **2014**, 631296.

[13] Ijspeert A J. Central pattern generators for locomotion control in animals and robots: A review. *Neural Networks*, 2008, **21**, 642–653.

[14] Yu J, Tan M, Chen J, Zhang J. A survey on CPG-inspired control models and system implementation. *IEEE Transactions on Neural Networks and Learning Systems*, 2014, **25**, 441–456.

[15] Zhang D, Hu D, Shen L, Xie H. A bionic neural network for fish-robot locomotion. *Journal of Bionic Engineering*, 2006, **3**, 187–194.

[16] Zhang D, Hu D, Shen L, Xie H. Design of an artificial bionic neural network to control fish-robot's locomotion. *Neurocomputing*, 2008, **71**, 648–654.

[17] Wu Z, Yu J, Tan M, Zhang J. Kinematic comparison of forward and backward swimming and maneuvering in a self-propelled sub-carangiform robotic fish. *Journal of Bionic Engineering*, 2014, **11**, 199–212.

[18] Li L, Wang C, Xie G. A general CPG network and its implementation on the microcontroller. *Neurocomputing*, 2015, **167**, 299–305.

[19] Yu J, Wu Z, Wang M, Tan M. CPG network optimization for a biomimetic robotic fish via PSO. *IEEE Transactions on Neural Networks and Learning Systems*, 2016, **27**, 1962–1968.

[20] Staffa M, Perfetto D, Rossi S. Engineering central pattern generated behaviors for the deployment of robotic systems. *Neurocomputing*, 2015, **170**, 98–112.

[21] Ge Q, Shao T, Yang Q, Shen X, Wen C. Multisensor nonlinear fusion methods based on adaptive ensemble fifth-degree iterated cubature information filter for biomechatronics. *IEEE Transactions on Systems*, *Man*, *and Cybernetics*: *Systems*, 2016, **46**, 912–925.

[22] Ge Q, Shao T, Chen S, Wen C. Carrier tracking estimation analysis by using the extended strong tracking filtering. *IEEE Transactions on Industrial Electronics*, 2017, **64**, 1415–1424.

[23] Yu J, Chen S, Wu Z, Wang W. On a miniature free-swimming robotic fish with multiple sensors. *International Journal of Advanced Robotic Systems*, 2016, **13**, 1–8.

[24] Yu J, Wang L, Tan M. Geometric optimization of relative link lengths for biomimetic robotic fish. *IEEE Transactions on Robotics*, 2007, **23**, 382–386.

[25] Wang W, Gu D, Xie G. Autonomous optimization of swimming gait in a fish robot with multiple onboard sensors. *IEEE Transactions on Systems*, *Man*, *and Cybernetics*: *Systems*, 2017, 1–13 (Article in press, https://doi.org/10.1109/TSMC.2017.2683524).

[26] Li L, Lv J, Chen W, Wang W, Zhang X, Xie G. Application of Taguchi method in the optimization of swimming capability for robotic fish. *International Journal of Advanced Robotic Systems*, 2016, **13**, 102.

[27] Deng F, Guo S, Zhou R, Chen J. Sensor multifault diagnosis with improved support vector machines. *IEEE Transactions on Automation Science and Engineering*, 2017, **14**, 1053–1063.

[28] Ji Z, Yu H. A new perspective to graphical characterization of multiagent controllability. *IEEE Transactions on Cybernetics*, 2017, **47**, 1471–1483.

[29] Othman A, Belda K, Burget P. Physical modelling of energy consumption of industrial articulated robots. *Proceedings of* 15*th International Conference on Control*, *Automation and Systems*, Busan, Korea, 2015, 784–789.